

# Nanoscale

Accepted Manuscript



This is an *Accepted Manuscript*, which has been through the Royal Society of Chemistry peer review process and has been accepted for publication.

*Accepted Manuscripts* are published online shortly after acceptance, before technical editing, formatting and proof reading. Using this free service, authors can make their results available to the community, in citable form, before we publish the edited article. We will replace this *Accepted Manuscript* with the edited and formatted *Advance Article* as soon as it is available.

You can find more information about *Accepted Manuscripts* in the [Information for Authors](#).

Please note that technical editing may introduce minor changes to the text and/or graphics, which may alter content. The journal's standard [Terms & Conditions](#) and the [Ethical guidelines](#) still apply. In no event shall the Royal Society of Chemistry be held responsible for any errors or omissions in this *Accepted Manuscript* or any consequences arising from the use of any information it contains.

# Rapid Capillary Filling via Ion-Water Interactions Over Nanoscale

Chirodeep Bakli and Suman Chakraborty\*

Department of Mechanical Engineering, Indian Institute of Technology Kharagpur, Kharagpur  
721302, INDIA.

Nanoscale Accepted Manuscript

**Corresponding Author** SC\* (email: [suman@mech.iitkgp.ernet.in](mailto:suman@mech.iitkgp.ernet.in))

**ABSTRACT**

Giant frictional resistances are grand challenges against the rapid filling of nanoscale capillaries, as encountered in a wide variety of applications ranging from nature to energy. It is commonly believed that partially wettable charged nano-capillaries fill up considerably slower, as compared to completely wettable ones, under the influence of a complex interplay between interfacial tension and electrical interactions. In sharp contrast to this common belief, here we discover a new non-intuitive regime of rapid filling of charged capillaries over nanometer scales, by virtue of which a partially wettable capillary may fill up comparatively faster than a completely wettable one. We attribute the fundamental origin of this remarkable behavior to ion-water interactions over interfacial scales. The underlying novel electro-hydrodynamic mechanism, as unveiled here, may provide deeper insights on the physico-chemical interactions leading to augmentations in the rates of nanocapillary filling over hydrophobic regimes, bearing far-reaching implications in the transport of biological fluids, enhanced oil recovery, and miniaturized energy harvesting applications.

## Introduction

Filling of nanoscale capillaries is an essential feature in a wide variety of biological, physical, and industrial applications, such as enhanced oil recovery<sup>1</sup>, mixing and separation<sup>2-4</sup>, anti-fouling systems<sup>5</sup>, rapid and point-of-care bio-medical research<sup>6,7</sup>, precise drug delivery<sup>8,9</sup>, desalination<sup>10</sup> and miniaturized energy conversion systems<sup>11,12</sup>. It is classically believed that the dynamics of such capillary filling processes is primarily dictated by interplay between driving surface tension and resistive viscous retardation mechanisms<sup>13-15</sup>. Over nanometer dimensions, interactions between these two forces are often mediated by the slippage of liquid over the solid boundaries<sup>16-20</sup>, which is intrinsic to fluid-fluid and fluid-solid interactions over small scales<sup>21</sup>.

In the presence of ionic inclusions in the fluid, an additional forcing mechanism influencing the capillary filling process comes into play<sup>22-24</sup>. Primary origin of this mechanism has its inception in the formation of an electrically charged interfacial layer at the solid boundary, leading to surplus ionic species of opposite charge in the bulk fluid<sup>25</sup>. Under the action of a driving interfacial tension, the surplus ionic species in the bulk gets preferentially transported towards the capillary meniscus. This, in turn, leads to the spontaneous development of a dynamically evolving induced axial back-electric field, despite no electrical voltage being externally applied<sup>26</sup>. The fluid interface boundary conditions like the boundary slip are known to drastically change with polarity and magnitude of surface charge<sup>27</sup> and presence of electric fields<sup>28</sup>. Under the action of this induced electric field, the meniscus may deform uniquely over nanometer scales, with a potential of influencing the capillary filling process in a rather non-intuitive manner.

Over microscale regimes, theoretical<sup>29,30</sup> and experimental studies<sup>31,32</sup> have revealed that the induced axial electric field across the filled portion of the capillary necessarily imposes a resistive influence. These effects are commonly known as electro-viscous retardation<sup>33</sup>, by drawing an analogy with an electrically modulated viscous damping mechanism. Such damping mechanisms are believed to slow down the capillary filling process to a considerable extent, with partially wettable capillaries trivially transmitting fluids slower as compared to completely wettable ones.

In sharp contrast to the intuitive understanding portrayed as above, we bring out hitherto-unveiled regime of amplified rate of capillary filling in a partially wettable nanochannel as compared to a completely wettable one. We arrive at this remarkable finding by capturing an intricate interconnection between interfacial slip and electrostatics, delving deep into ion-water interactions over nanometer scales. First, we execute molecular dynamics (MD) simulations to capture the dynamical evolution of a capillary filling process of an ionic solution over nanometer scales. Second, we derive a novel theoretical framework that captures the essential physics of interest revealed from our MD experiments. These results corroborate with the fact that the effect of intrinsic wettability of a capillary may indeed be altered by simply employing saline solutions of pre-determined concentrations. This opens up unprecedented rapid regimes of filling of partially wettable capillaries, bearing far ranging consequences in applications ranging from biomedical diagnostics to energy harvesting over nanometer scales.

### Simulation Details

We perform the MD simulations on a slit of 1.5 nm, connected to a reservoir having dimension of  $12 \times 12 \times 10$  nm. The reservoir is large enough to sustain the capillarity, while water imbibes into the slit. The initial density of water inside the reservoir is based on the density of water at 300K and hence, the reservoir, in this case, accommodates 48204 water molecules. In order to simulate saline solutions, sodium and chloride ions are randomly distributed in the fluid bulk. The formation of electrical double layer (EDL) is accounted for by assigning a uniformly distributed negative charge on the wall particles in contact with the fluid and maintaining the electro-neutrality by having less number of anions than cations. We also simulate a separate system with discrete charges on random wall particles mimicking charged group on the surface. However, our simulation system includes only atomically smooth surfaces, and the electric friction induced by protrusions from charged groups<sup>34,35</sup> is not accounted for. The results from the two sets of simulations do not demonstrate any discernable difference<sup>36,37</sup>. The results demonstrated here are obtained for a surface charge density of  $0.024 \text{ C} / \text{m}^2$ . This optimum value of surface charge allows physically realistic ion distribution for the formation of EDL and also do not severely attenuate slip lengths due to pinning of polar water molecules at charged surface sites. The simple point charge/extended (SPC/E)<sup>38</sup> model for water is used. The wall atoms are modeled Lennard-Jones (LJ) particles. The intrinsic wettability of the surface is varied by tuning

the LJ parameters of the wall atoms which alters the van der Waals interactions between the wall and water molecules. The homo-nuclear LJ parameters of the wall particles are varied as  $\epsilon_{ww}$  ranges from  $2.5 \text{ kJ/mol}$  to  $6 \text{ kJ/mol}$ , and  $\sigma_{ww} = 0.35 \text{ nm}$  is kept fixed for the simulations while the hetero-nuclear LJ interactions are obtained using standard mixing rules<sup>39</sup>. The dynamic evolution of the meniscus position is observed by tracking the density distribution of water molecules in the slit.

The velocity profiles are obtained after binning the flow in the channels done by averaging the individual molecular velocities. These velocity profiles form the basis of determining the slip length of water in flow<sup>17,40</sup>. The extrapolated velocity profile, in accordance with Navier slip considerations,  $u_s = l_s \left. \frac{du}{dy} \right|_b$ , gives the slip length  $l_s$ ,  $\left. \frac{du}{dy} \right|_b$  being the wall-normal velocity gradient.

## Results and Discussion

**Non monotonic dependence of capillary filling rate on salt concentration: interplay of electro-viscous interactions.** We first execute MD simulation experiments (Methods) to analyze the filling behavior in charged capillaries conveying salted solutions of various concentrations (for a schematic depiction of the domain, see figure 1). The presence of microions in water and the surface charge at the walls leads to the development of a charged interfacial layer, also known as the electrical double layer (EDL). Ions in the diffuse part of this EDL are preferentially transported and redistributed in a dynamically evolving environment, under a driving Laplace pressure gradient originating out of interfacial tension. This redistribution leads to the dynamic evolution electromigration current of ions, opposing the streaming current. The induced streaming potential across the axial extent of the meniscus, in effect, tends to oppose the imbibition of fluid into the capillary, with an intuitive slowing down of the capillary front due to electro-viscous action<sup>33</sup>. However, the rearrangement of the ionic inclusions in the fluid induces considerable local fluctuations in the fluid density, viscosity and other properties. This renders the capillary filling dynamics a more complex process than what may be intuitively portrayed.

We first present the square of the filling-length of completely wettable charged nanoscale capillaries as a function of time, for different salt concentrations (Figure 2). We observe that the

filling rates are slower than uncharged capillaries conveying pure water (with perfectly wettable capillaries considered in all scenarios), as an intuitive consequence of electro-viscous retardation. However, contrary to intuition, the variation of filling rate with salt concentration is observed to be non-monotonous. First, the filling rates tend to increase with rise in salt concentration. With further increase in salt concentration, filling rates start decreasing. For concentrations beyond  $1 M$ , filling rates are observed to decline rapidly. To track the non-monotonous variation of filling rate with salt concentration, we plot the height of the meniscus attained at  $time = 3 ns$  for various salt concentrations (inset of figure 2). Maximum filling rate is observed around a concentration of  $0.5 M$ . It is interesting to note that one may find an analogy of this aspect of the charged capillary filling with two seemingly unrelated physical scenarios. First, the measurement of zeta potential for electrokinetic transport in a liquid film covered with ionic surfactants may be referred. The zeta potential first increases and then decreases with decrease of surfactant coverage<sup>41</sup>. The zeta potential over a hydrophobic surface is believed to generate giant electrokinetic effects<sup>42</sup> and can also lead to non-monotonic frictional behavior on a hydrophilic surface under certain circumstances. Researchers have attributed the dynamics at the liquid-air interface and the ion binding mechanism for the observed zeta potential maxima at intermediate surface coverage. The second example comes from the variation of electrokinetic energy conversion efficiency characteristics of nanofluidic channels, which exhibit a similar non-monotonic trend with the surface charge density<sup>43</sup>. Drawing an analogy from the aforementioned results, we can infer that the introduction of ions in capillary leads to a competition between the electroviscous forces and the hydrodynamic viscous resistance, with a salt concentration-dependent interplay.

**Filling of partially wettable nanocapillaries at low salt concentrations.** We capture the contact angle dependence of the observed phenomenon for low salt concentrations ( $\sim 0.1 M$  or less), within the hydrophilic regime (shown in fig. 3). The filling rates, quite intuitively, increase with increase in wettability. It is worth noting that even for a moderately hydrophilic surfaces (for example the demonstrated contact angles of  $46^\circ$  and  $65^\circ$  in fig. 3) the capillary filling occurs pretty rapidly, so that the completely wettable and partially wettable capillaries have filling rates that do not exhibit any appreciable difference for low salt concentrations.

The observed trends may be nicely explained by devising a simple yet insightful theoretical consideration. This may be realized by working a balance of the forces due to the Laplace pressure gradient ( $F_{lap}$ ) across the meniscus, viscous drag ( $F_{vis}$ ), and electrokinetic interaction force ( $F_e$ ), leading to  $F_{vis} + F_e + F_{lap} = 0$ . Expressions  $F_{vis}$  and  $F_{lap}$  may be worked out in a straight forward manner (see ESI). Expression for The electrokinetic force may be estimated as:  $F_e = q_p E_s$ , where  $q_p$  is the net free charge in the solution (contributed by the dissolved ionic species in the fluid), and  $E_s$  is the dynamically evolving streaming potential field established across the meniscus. With  $n_+$  and  $n_-$  as the cationic and anionic densities respectively in the capillary, the free charge per unit channel width, for a z:z symmetric electrolyte, following the Boltzmann distribution<sup>26</sup>, is  $q_p = L \int_{-H}^H ze(n_+ - n_-) dy = -\frac{4n_o L z^2 e^2 \zeta \lambda}{k_B T} \tanh(H / \lambda)$ , where  $e$  is the protonic charge,  $z$  the valance of ion,  $k_B$  is the Boltzmann constant,  $T$  is the absolute temperature,  $n_o$  is the ion density in the bulk,  $H$  is the half-height of the slit,  $\zeta$  is the zeta potential, and  $\lambda$  is the Debye length given by the expression  $\lambda = \sqrt{\frac{\epsilon k_B T}{2n_o e^2 z^2}}$ ;  $\epsilon$  being the permittivity of the fluid<sup>25,26</sup>. In an effort to determine  $E_s$ , we need to obtain the velocity field (from the Stokes equation with a dynamically evolving electrical body force term), closed by the constraint of zero net ionic current<sup>44</sup> as attributable to the absence of any externally applied electric field (for details, see ESI).

In order to rationalize the theoretical findings vis-a-vis the interfacial phenomena over molecular scales, we consider slip velocity over the confining boundaries of the fluidic capillary. While this is not a new proposition over nanometer scales<sup>45</sup>, we make an additional consideration here by invoking that the slip lengths observed must be manifestations of the coupled action of hydrodynamic and electrokinetic influences over interfacial scales. In other words, we consider the hydrodynamic and electrokinetic components of the slip velocities at the wall to be contributing, in combination, to the net interfacial slip velocity. This leads the following expression for the dynamically induced streaming potential field across the capillary meniscus (for derivation, see ESI):

$$E_s = \frac{\frac{\zeta\gamma\lambda^2}{\eta L} \cos\theta \left( \frac{\lambda}{H} \tanh(H/\lambda) - 1 \right) - \zeta u_s \lambda \tanh(H/\lambda)}{\frac{k_B T H}{f} + \frac{\varepsilon \zeta^2}{2\eta} \left( \lambda \tanh(H/\lambda) - \frac{H}{(\cosh(H/\lambda))^2} \right)}, \quad \text{where } u_s = u_{sp} + u_{se}. \quad \text{Here}$$

$$u_{sp} = \left( \frac{\gamma \cos\theta}{HL} \right) \left[ \frac{(H^2 - y^2)}{2\eta} + \frac{(l_{sp}/H)}{\eta} H^2 \right]_{wall} \quad \text{and}$$

$$u_{se} = \left( \frac{\varepsilon E_s \zeta}{\eta} \right) \left[ \frac{\cosh(y/\lambda)}{\cosh(H/\lambda)} - 1 + \frac{l_{se}}{\lambda} \tanh(H/\lambda) \right]_{wall}, \quad \text{where } l_{se} \text{ is the slip length of the}$$

electrokinetically driven flow component and  $l_{sp}$  is the slip length for the Laplace pressure gradient driven flow component. Here,  $l_{se}$  and  $l_{sp}$  are mere artificially defined quantities which indicate the sole contribution of electrostatic and hydrodynamic forces, respectively. On combining these two parameters based on the Navier slip model relating wall shear stress with the tangential velocity jump, the actual boundary slip is obtained (for details, see ESI). The variation of slip length under the influence of static and mobile charges agrees with the observations of Joly et al.<sup>42</sup>

In an effort to obtain insights on the trends of capillary filling dynamics observed in Fig. 3, the wettability-dependence of total slip length, for saline water solution having concentration of  $0.1 M$ , is shown in the inset, as obtained from independent MD experiments for flows through nanochannels of prescribed wettability values. Although,  $l_{se}$  cannot be explicitly determined from direct MD simulations,  $l_{sp}$  is determined from a purely pressure driven flow where streaming potential is not allowed to build-up<sup>17,40</sup>. By assuming linear superposition of the slip velocities (not slip lengths),  $l_{se}$  can be determined. The resultant slip length values obtained here are not mere summations of  $l_{sp}$  and  $l_{se}$ . The net slip length,  $l_s$ , can be determined from the relationship between the slip velocity and the wall normal velocity gradient for the resultant flow velocity (a linear superposition of the two velocity components).

At low enough solute concentrations,  $l_s$  is observed to be positive throughout the range of wettabilities chosen in the simulations. This indicates a recessive electrokinetic slip/stick at

lower concentrations, irrespective of the wettability. The absence of fluid stick at the boundary may be attributed to the fact that less numbers of charged species occupy the interfacial region at low bulk concentrations. Accordingly, the possibilities of the formations of hydration shells by the interfacial ions and the associated pinning the wall-adjacent water molecules remain inconsequential. Another interesting inference obtained by comparing the individual slip length values is that while  $l_{se}$  is a strong function of the salt concentration and surface charge, i.e. the electrokinetic parameters,  $l_{sp}$  strongly varies with the wettability and the other hydrodynamic parameters. Taking the statistical fluctuations in the simulation results into account, we can consider  $l_{sp}$  to be independent of surface charge and salt concentration. Similarly,  $l_{se}$  is independent of the wall wettability. This inference is in agreement with the filling dynamics observed at low salt concentrations.

Using this slip length data, it is revealed that our theoretical calculations agree excellently with the MD simulation data on instantaneous capillary filling length (see Fig. 3). The occurrence of fluid slip over the entire spectrum of partially wettable pores at low solute concentrations tends to enhance the capillary filling rate. A detailed observation of the force balance equation reveals that a large value of  $l_{sp}$  would reduce the viscous force opposing the capillary filling. This slip, being wettability dominated, drastically increases for partially wettable pores. Hence, irrespective of the declining  $\cos\theta$  values, the decreasing Laplace pressure aiding capillarity is compensated by the decreasing viscous resistance due to enhanced slip at lower wettabilities. This causes the filling rates not to drastically decline for partially wettable pores as observed for unsalted water, although the filling rates of partially wettable pores remain slower as compared to that for completely wettable ones, at low salt concentrations.

**Rapid filling of charged capillaries at high salt concentrations: effective hydrophilization of partially wettable channels.** For higher salt concentrations ( $\sim 1$  M or more), we observe a remarkable and non-intuitive phenomenon in a sense that the capillary filling rate through partially wettable charged nanopores is found to appreciably more rapid as compared to that of completely wettable ones. For example, water fills a nanochannel with contact angle of  $46^\circ$

faster than a completely wettable nanochannel at a salt concentration of  $1.5 M$  ( figure 4). Irrespective of the fact that the driving capillary force for a partially wettable channel is less than a completely wettable one, the opposite capillary filling trend observed can be attributed to the coupled nature of slip and surface charge<sup>43,46</sup>. In the presence of surface charging, the ions tend to form hydration shells, pinning a layer of interfacial water. The surrounding water molecules tend to have a compensated hydrogen bonding network and tend to agglomerate around the primary hydration shells<sup>47</sup>. This alters the polarizability of the fluid at the interface and hence the interfacial fluid friction<sup>14,48,49</sup>. This leads to electrokinetic stick, and hence negative values of the electrokinetic slip length,  $l_{se}$ . Further,  $l_{se}$  declines rapidly with increase in salt concentration, due to enhanced pinning of interfacial water owing to the increased surface density of ions. However, the Laplace pressure driven slip length component,  $l_{sp}$ , is insensitive to the salt concentration, especially bearing high values for lower wettabilities. As observed for a solute concentration of  $1.5 M$  here, the total slip length remains negative for contact angles below  $50^\circ$ . Only further decrease in wettabilities produces positive net slip length  $l_s$ , indicating dominance of hydrodynamic slip over electrokinetic stick. Comparing the viscous drag forces in pores of varying wettabilities, with the considerations of the respective slip length components (see inset of fig. 4), indicates lower viscous resistances in partially wettable pores. However, a lower viscous drag is not sufficient to induce accelerated filling in capillaries of lower wettabilities. Intriguingly, examination of the electrical force,  $F_e$ , reveals a three way modulation of the electro-viscous force due to the non-additive and mutually independent properties of the slip length components  $l_{sp}$  and  $l_{se}$ , as well as the wettability dependent driving force (proportionality with  $\cos \theta$ ). It is of interest to note that the zone where the maximum filling rate augmentation is obtained has the electrokinetic and hydrodynamic slip lengths with opposite signs. For superhydrophilic capillaries, slip lengths are small and do not counter the effect of electroviscous retardation. On the other hand, for capillaries having wettability with equivalent static contact angle close to  $90^\circ$ , the filling rates are extremely small as boundary slip is insufficient to augment filling rates due to debilitated Laplace pressure term. It is the moderately hydrophilic zone, where considerable filling rate enhancement occurs.

A high positive value of  $l_{sp}$  would lead to lower value of the numerator of the expression for  $E_s$ . On the other hand, increased electrokinetic stick would not have appreciable effect on the magnitude of the denominator of the same. The low values of Debye length,  $\lambda$ , pertinent to highly concentrated solutions, would imply the second term in the denominator to be much smaller than the first term. In addition,  $E_s$  also scales linearly with the  $\cos\theta$ , rendering an explicit wettability-dependence to the electrokinetic influences. Thus, partially wettable pores are subject to lower opposing electrical force as compared to completely wettable ones, all other conditions remaining unaltered. Hence, partially wetting pores carrying concentrated salt solutions have the balance of the reduced aiding capillary force and the reduced opposing force due to the streaming potential field combined, so as to yield augmented filling speeds, as compared to completely wettable ones. Remarkably, this results in the inception of a new regime in which the capillary filling rate is conflicting to that dictated by its intrinsic wettability. With an effective interplay of electro-chemico-hydrodynamic interactions over interfacial scales, such a hydrophilization at high salt concentrations may be observed. This is physically non-intuitive, which we pinpoint as the regime of hydrophilization of partially wettable channels, bearing tremendous consequences in biological and energy applications over nanometer scales.

For a unified understanding of the meniscus dynamics under the viscous and the electrokinetic forces, we need to appreciate the fact that the interfacial dynamics for the two forcing mechanisms intrinsically differs. In other words, the degree of interfacial slippage, the mechanism causing slip, and the manifestation of slip through the differently shaped velocity profiles are completely different for electrokinetic and pressure driven flows. This fact leads to the counter-intuitive acceleration and retardation of the meniscus for different solute concentrations and substrate wettabilities. Thus, in most cases, the capillary retardation caused by the electro-viscous forces is partly compensated by the reduction in viscous drag due to slip at the walls.

Along with the continuum picture, a molecular explanation for the observed behavior for higher salt concentration can be obtained. In the simulations, we vary the salt concentration, keeping the surface charge density constant. The number density of counter ions next to the

surface is expressed as  $n_s = n_o + \frac{\Sigma^2}{2\epsilon k_B T}$ , where  $\Sigma = 0.024C / m^2$ , the surface charge density in

our simulations. Thus, in the simulation domain, the counter-ion number density next to wall comes to about  $10^{27}$ , which implies approximately a counter-ion concentration of  $1.66 M$  next to the wall. Hence, for a dilute salt solution (say  $0.5 M$ ), there is considerable segregation of ions across the channel, with the centerline having minimum concentration and the walls having maximum. This sets up a flow of water molecules towards the wall. This cross-axial flow of water increases the curvature of the meniscus and thus diminishes the traction force leading to retardation to capillarity. However, for higher concentration, the cross-axial flow is considerably less due to more uniform distribution of ions across the cross-section. In such a case, slippage at the wall would further enhance this effect and thus the reversal is observed in fig. 4; a completely wettable pore has lower filling rates than partially wettable ones.

## Conclusions

To summarize, we demonstrate that with a novel interplay of electrical and hydrodynamic forces over interfacial scales, as mediated by a salted solution of high concentration, partially wettable nanochannels may fill up remarkably faster as compared to completely wettable ones. We also provide a molecular level description of the mechanism causing such non-intuitive effective wettability for charged capillaries carrying concentrated salt solutions, opening up new regimes of rapid capillary filling over nanometer scales. The mechanism underlying this unexplored behavior can be exploited for amplifications in the rates of propulsion of ionic solution and biological fluids through naturally occurring and in-vitro hydrophobic nanopores in diverse applications ranging from biological sciences to energy harvesting.

## Acknowledgements

The authors gratefully acknowledge Sponsored Research and Industrial Consultancy cell, IIT Kharagpur, for financial support through the Projects “Centre of Excellence for Training and Research in Microfluidics”, and “Point of Care Diagnostics”

Additional details available in ESI.

## REFERENCES

1. H.-Q. Sun, L. Zhang, Z.-Q. Li, L. Zhang, L. Luo, and S. Zhao, *Soft Matter*, 2011, **7**, 7601.
2. M. Tani, R. Kawano, K. Kamiya, and K. Okumura, *Sci. Rep.*, 2015, **5**, 10263.
3. L.-P. Xu, B. Dai, J. Fan, Y. Wen, X. Zhang, and S. Wang, *Nanoscale*, 2015, **7**, 13164–13167.
4. W. Zhang, X. Lu, Z. Xin, and C. Zhou, *Nanoscale*, 2015, **7**, 19476–19483.
5. F. Xia, H. Ge, Y. Hou, T. Sun, L. Chen, G. Zhang, and L. Jiang, *Adv. Mater.*, 2007, **19**, 2520–2524.
6. S. Hernández-Ainsa and U. F. Keyser, *Nanoscale*, 2014, **6**, 14121–14132.
7. M. Chehel Amirani and T. Tang, *Nanoscale*, 2015, **7**, 19586–19595.
8. A. Allen and N. J. H. Carroll, *Dig. Dis. Sci.*, 1985, **30**, 55S–62S.
9. G. Fullstone, J. Wood, M. Holcombe, and G. Battaglia, *Sci. Rep.*, 2015, **5**, 10649.
10. Y. You, V. Sahajwalla, M. Yoshimura, and R. K. Joshi, *Nanoscale*, 2015.
11. H. Daiguji, P. Yang, A. J. Szeri, and A. Majumdar, *Nano Lett.*, 2004, **4**, 2315–2321.
12. F. H. J. van der Heyden, D. J. Bonthuis, D. Stein, C. Meyer, and C. Dekker, *Nano Lett.*, 2007, **7**, 1022–5.
13. J. F. Joanny and P. G. de Gennes, *J. Chem. Phys.*, 1984, **81**, 552.
14. F. B.-W. P.G. de Gennes, *Capillarity and Wetting Phenomena: Drops, Bubbles, Pearls, Waves*, Springer, New York, 2003.
15. J. . Rowlinson and B. Widom, *Molecular theory Of Capillarity*, Cambridge University Press, 2000.
16. D. I. Dimitrov, A. Milchev, and K. Binder, 2007, **054501**, 1–4.
17. C. Bakli and S. Chakraborty, *Appl. Phys. Lett.*, 2012, **101**, 153112.
18. C. Lee, C.-H. Choi, and C.-J. ‘CJ’ Kim, *Phys. Rev. Lett.*, 2008, **101**, 064501.
19. C. Bakli and S. Chakraborty, *Nano Lett.*, 2015, **15**, 7497–7502.
20. C. Bakli and S. Chakraborty, *Soft Matter*, 2015, **11**, 161–168.

21. V. Janeček, B. Andreotti, D. Pražák, T. Bárta, and V. Nikolayev, *Phys. Rev. E*, 2013, **88**, 060404.
22. P. Lo Nostro and B. W. Ninham, *Chem. Rev.*, 2012, **112**, 2286–2322.
23. P. Jungwirth and D. J. Tobias, *Chem. Rev.*, 2006, **106**, 1259–1281.
24. Y.-P. Zhao and Q. Yuan, *Nanoscale*, 2015, **7**, 2561–2567.
25. R. J. Hunter, *Zeta Potential in Colloid Science: Principles*, Academic Press, 1981.
26. R.F. Probstein, *Physicochemical Hydrodynamics: An Introduction*, Wiley-Interscience, New York, 1994.
27. Y. Pan and B. Bhushan, *J. Colloid Interface Sci.*, 2013, **392**, 117–21.
28. Y. Pan, B. Bhushan, and X. Zhao, *Beilstein J. Nanotechnol.*, 2014, **5**, 1042–1065.
29. V.-N. Phan, C. Yang, and N.-T. Nguyen, *Microfluid. Nanofluidics*, 2009, **7**, 519–530.
30. S. Das, S. Chanda, J. C. T. Eijkel, N. R. Tas, S. Chakraborty, and S. K. Mitra, *Phys. Rev. E*, 2014, **90**, 043011.
31. N. R. Tas, J. Haneveld, H. V. Jansen, M. Elwenspoek, and A. van den Berg, *Appl. Phys. Lett.*, 2004, **85**, 3274.
32. F. Persson, L. H. Thamdrup, M. B. L. Mikkelsen, S. E. Jaarlgard, P. Skafte-Pedersen, H. Bruus, and A. Kristensen, *Nanotechnology*, 2007, **18**, 245301.
33. S. Levine, J. . Marriott, G. Neale, and N. Epstein, *J. Colloid Interface Sci.*, 1975, **52**, 136–149.
34. Y. W. Kim and R. R. Netz, *Europhys. Lett.*, 2005, **72**, 837–843.
35. Y. W. Kim and R. R. Netz, *J. Chem. Phys.*, 2006, **124**, 114709.
36. D. Ben-Yaakov, D. Andelman, and H. Diamant, *Phys. Rev. E. Stat. Nonlin. Soft Matter Phys.*, 2013, **87**, 022402.
37. F. Jiménez-Ángeles, *Phys. Rev. E. Stat. Nonlin. Soft Matter Phys.*, 2012, **86**, 021601.
38. H. J. C. Berendsen, J. R. Grigera, and T. P. Straatsma, *J. Phys. Chem.*, 1987, **91**, 6269–6271.
39. M. P. Allen and D. J. Tildesley, *Computer Simulation of Fluids*, Clarendon Press, 1987.
40. C. Bakli and S. Chakraborty, *J. Chem. Phys.*, 2013, **138**, 054504.
41. L. Joly, F. Detcheverry, and A.-L. Biance, *Phys. Rev. Lett.*, 2014, **113**, 088301.
42. L. Joly, C. Ybert, E. Trizac, and L. Bocquet, *J. Chem. Phys.*, 2006, **125**, 204716.

43. C. Bakli and S. Chakraborty, *Electrophoresis*, 2015, **36**, 675–681.
44. S. Chakraborty and S. Das, *Phys. Rev. E*, 2008, **77**, 037303.
45. W. Sparreboom, A. van den Berg, J. C. T. Eijkel, H. Search, C. Journals, A. Contact, and M. Iopscience, *New J. Phys.*, 2010, **12**, 015004.
46. S. Chakraborty, D. Chatterjee, and C. Bakli, *Phys. Rev. Lett.*, 2013, **110**, 184503.
47. A. Boğan, V. Marry, B. Rotenberg, P. Turq, and B. Noetinger, *J. Phys. Chem. C*, 2013, **117**, 978–985.
48. C. Wang, B. Wen, Y. Tu, R. Wan, and H. Fang, *J. Phys. Chem. C*, 2015, **119**, 11679–11684.
49. G. Tocci, L. Joly, and A. Michaelides, *Nano Lett.*, 2014, **14**, 6872–7.

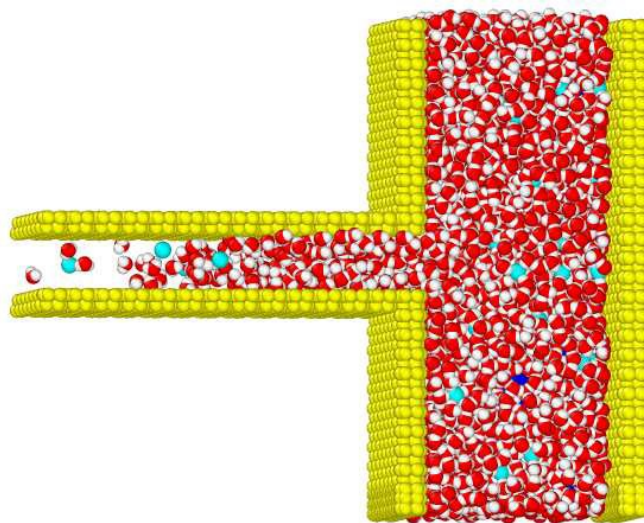


**Figure 1.** An explored view of the domain. Reservoir containing water with dissolved NaCl is connected to the slit into which the fluid imbibes. The cyan particles are  $\text{Na}^+$  ions and blue particles are  $\text{Cl}^-$  ions.

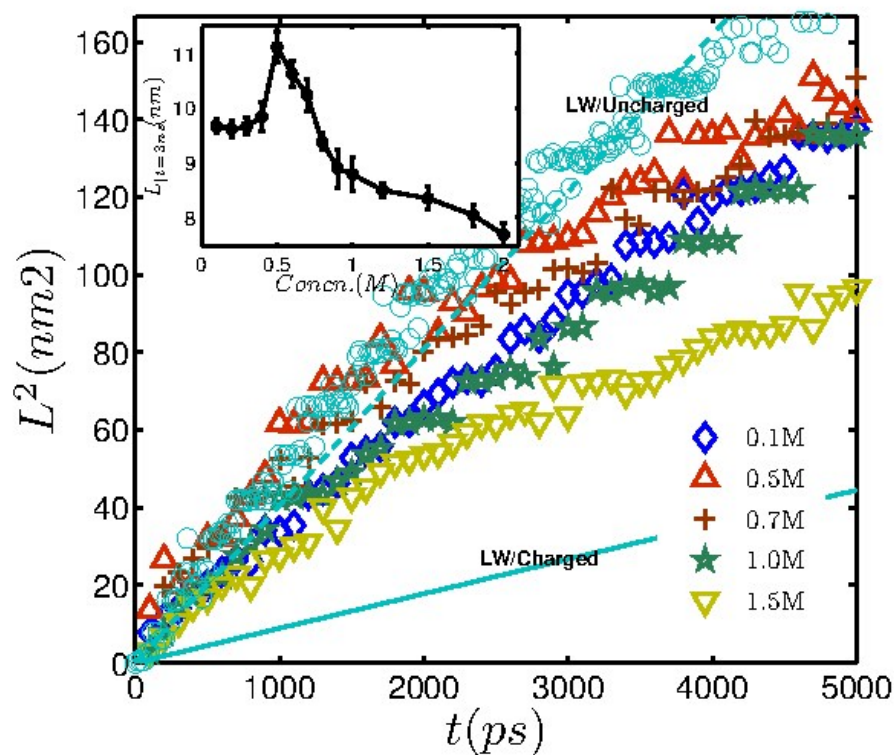


**Figure 2.** Squares of filling lengths of completely wettable charged nanoslits carrying saline solutions of different concentrations. The capillary filling data obtained by averaging the simulation results reveal slower filling rates in charged capillaries as compared to the filling rates observed in uncharged pores or the constant slope predicted by traditional Lucas Washburn (LW) analysis at similar scales. The dashed line represents the LW analytical curve and the circles represent the MD data for an uncharged channel with pure water and the bold line represents the filling rate in charged channels obtained from classical LW analysis with electroviscous retardation. The plot at the inset depicts the filled length at  $t = 3 \text{ ns}$  for various salt concentrations. As opposed to an intuitive electro-viscous retardation-induced monotonic slowing down of capillary filling at all salt concentrations, a non-monotonous variation is observed.

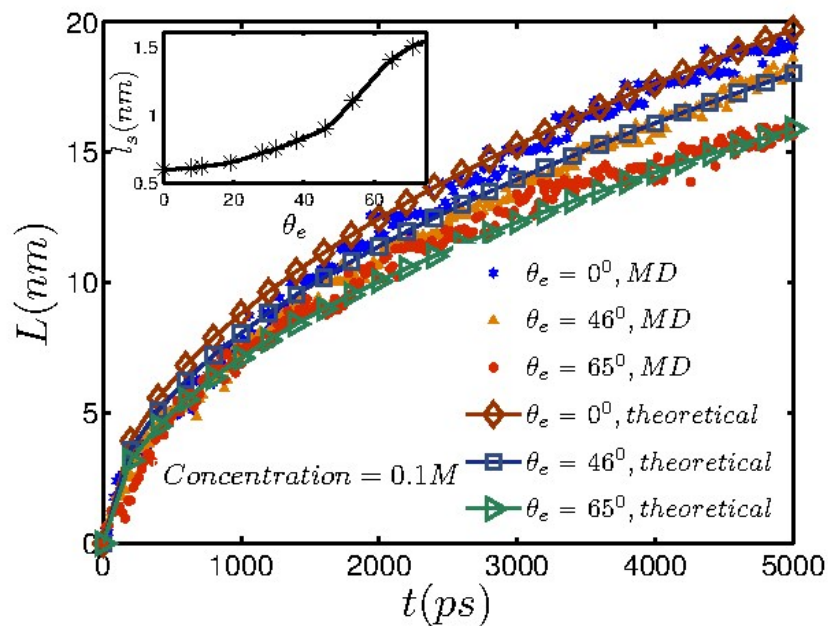


**Figure 3.** The filling distance as a function of time for capillaries with wettabilities equivalent to static contact angles ( $\theta$ ) of  $0^\circ$ ,  $46^\circ$  and  $65^\circ$ , at a low salt concentration ( $0.1 M$ ). The markers represent the MD simulation data. The continuous lines depict the results obtained from the theoretical model. Inset shows the slip length variation with contact angle obtained for the same concentration and surface charge.

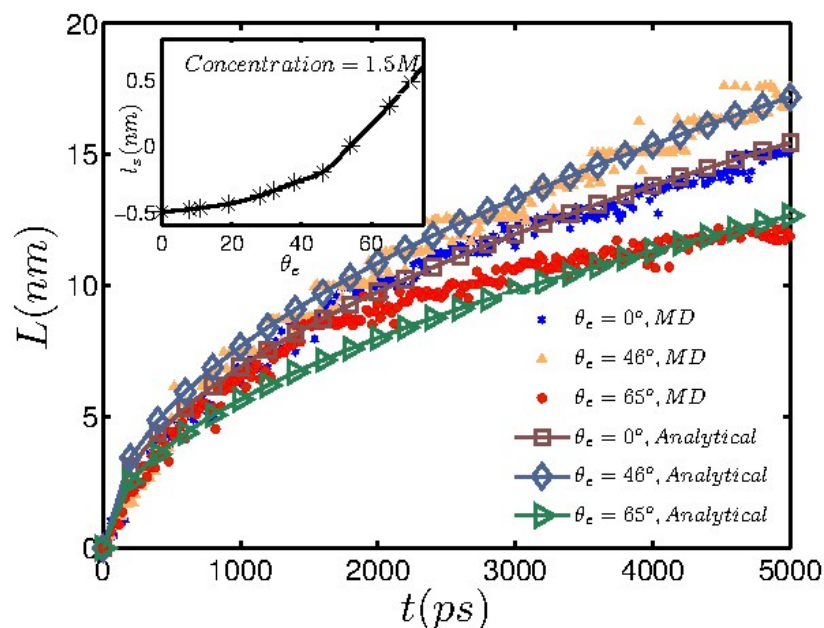


**Figure 4.** The instantaneous filling lengths of capillaries with varying wettabilities at high salt concentration (1.5 M). Completely wettable pores do not show the maximum filling speeds. The driving surface tension force decreases with wettability and so does the viscous force. However, the opposing electrokinetic force shows a greater decrease leading to rapid filling in partially wettable pores, as compared to completely wettable ones (for comparison with the theoretical LW equation with electroviscous retardation see ESI). Inset shows the slip length variation under identical flow conditions in independent MD simulations.